American Mineralogist, Volume 60, pages 758–770, 1975

High Resolution Electron Microscopy of Enstatite I: Twinning, Polymorphism, and Polytypism

SUMIO IIJIMA,

Department of Physics

AND PETER R. BUSECK

Departments of Geology and Chemistry

Arizona State University, Tempe, Arizona 85281

Abstract

All of the Ca-poor pyroxenes that we have examined contain coherent, intimate intergrowths of orthorhombic enstatite (OREN) and monoclinic enstatite (CLEN). We confirm that the relationship between these polymorphs can be explained in terms of unit cell twinning. Theoretically, such twinning can also give rise to a number of enstatite polytypes. During the martensitic CLEN→OREN transformation the bounding Si(*A*) chains are severely strained, but Si–O bonds are not broken. This is not the case for the octahedral sites, where foreign cations may enter and stabilize the structure. The partial dislocations are parallel to [011] at the incoherent OREN-CLEN boundaries.

Introduction

In our earlier paper (Buseck and Iijima, 1974) we explored the applications of a new mineralogical technique, high resolution electron microscopy, to the study of the main silicate mineral groups. Although some attention was given to deviations from ideality, the main emphasis was the imaging of perfect or nearly perfect crystals. In this and the subsequent paper (Buseck and Iijima, 1975) we wish to explore certain deviations from ideal structures and perfect periodicities.

More specifically, this paper has a double goal: (1) to explore the significance and ramifications of twinning as interpretable by electron microscopy, and (2) to investigate the nature of pyroxene polymorphism, a situation where two crystal structures intergrow coherently on a unit cell scale. Emphasis will be placed on the character of pyroxene, particularly enstatite, but the abundance and significance of twinning, a widespread and important phenomenon in many minerals, will be apparent throughout.

Pyroxenes are major terrestrial and extraterrestrial rock-forming minerals. The nature and interrelationships of the enstatite polymorphs have been a subject of intense investigation as well as controversy. The interrelationships potentially bear on recent work extending the use of enstatite for geothermometry (Warner and Luth, 1974) and geobarometry (MacGregor, 1974).

Of the three well recognized enstatite polymorphs —protoenstatite (PEN)[1], orthoenstatite (OREN)[1] and low clinoenstatite (CLEN)[1]—both OREN and CLEN can exist at room temperatures. OREN is more common in terrestrial rocks, whereas CLEN is abundant in many meteorites. Their stability relationships and structures have been reviewed by Smith (1969), Morimoto (1975), and Smyth (1974).

Single crystal X-ray structure determinations have been made of these polymorphs (Morimoto, Appleman, and Evans, 1960; Morimoto and Koto, 1969; Smyth, 1971). Streaking and diffuse spots or broad, blurred lines are common features of single crystal and powder diffraction patterns. These have been widely attributed to stacking faults and/or disorder. As detailed study of these features by X-ray techniques has been inadequate, we thought that electron microscopy might prove useful. There have been several other electron microscope studies of orthopyroxenes (Kohlstedt and Vander Sande, 1973; Coe and Müller, 1973; Lally *et al,* 1972; Boland, 1972; Champness and Lorimer, 1973, 1974; Vander Sande and Kohlstedt, 1974; Müller, 1974); most of

[1] We suggest these abbreviations as they are advantageous in terms of brevity, pronounciation, and mnemonics.

these papers describe geometrical features of the defects at lower resolutions than we consider, and primarily emphasize deformation and exsolution. We shall emphasize crystallographic relations as well as certain defects that are particularly amenable to high resolution microscopy. Preliminary results were presented by Iijima and Buseck (1973).

Experimental

Samples

Three types of specimens were used in this and the following paper (Buseck and Iijima, 1975): terrestrial enstatite from Bamble, Norway, and Papua, New Guinea; meteoritic enstatite from the Norton County, Shallowater, Bishopville and Steinbach meteorites (the last pyroxene is actually bronzitic); and synthetic enstatite crystallized from a gel. Because of the large amount available, most of the experiments were performed on a large (10 cm) single crystal of Bamble material having a well developed (100) parting. Microprobe analysis indicates the following composition (wt percent): FeO, 10.5; MgO, 32.6; CaO, 0.15; SiO_2, 56.7; and a formula $(Fe,Mg,Ca)_{2.024}\ Si_{1.990}O_6$. Compositionally, this makes this pyroxene a bronzite; we refer to it as enstatite for brevity, in accordance with other workers who have studied Bamble pyroxene.

Structurally, Bamble enstatite is the most pure OREN that we encountered. In order to obtain CLEN we heated the Bamble OREN as well as some Norton County and synthetic samples at 1000°, 1300°, or 1485°C for periods ranging from 12 to 168 hours.

Electron Microscopy

The samples were ground in an agate mortar, and dispersed in acetone. One drop of the suspension was collected on a perforated carbon film. Very thin crystallites were chosen and examined using an electron microscope equipped with a goniometer stage (JEM-100B) at 100 kV, as described previously (Buseck and Iijima, 1974).

The OREN-CLEN relationships can be observed most easily using *a-c* sections, *i.e.*, b^* coincident with the optical axis of the microscope. Because electron diffraction spots with l odd are forbidden, the $h0l$ reciprocal lattice row is absent, and the objective aperture (50 μm diameter) normally only includes beams from the $h00$ reciprocal lattice row, *i.e.*, OREN or CLEN with $h = \pm1, \pm2, \pm3, \pm4$. For the present purpose of studying the intergrowths of OREN and CLEN, it is sufficient to resolve the 9Å periodicities along a and it is not necessary to obtain the 'structure images' that require the severe imaging conditions reported previously (Buseck and Iijima, 1974). Thus, the present fringe images do not always show a direct correspondence with the structure, but do represent the (100) periodicities of the structure.

For some purposes it is advantageous to view *a-b* sections, *i.e.*, with c^* coincident with the electron beam. The relationship between OREN and CLEN is easily seen, as is the shifting of twin planes.

Grinding Artifacts

In considering the microscopic features of enstatite it is important to distinguish between original features and those introduced during sample preparation, primarily grinding. The main material that we studied was Bamble enstatite, and in many instances we heated the samples in the laboratory in order to produce CLEN from OREN. It is such samples, predominantly CLEN, that we discuss in this section (procedures for distinguishing the polymorphs are discussed below).

In some instances, during crushing of previously heated samples the crystals will fracture roughly parallel to (100). Along the fracture surface in a few samples we have noticed the initiation of unit cell twinning extending into the grain. These twin zones are indistinguishable in detail from those that presumably existed prior to our sample treatment. The only difference is that the original planes extend far into and generally through the crystals rather than being localized near the grain edges. Although this is a difference in degree rather than kind, we believe that the difference in development is sufficiently pronounced that we can distinguish between the two types with a relatively high degree of confidence.

Structural Relations

Basic Structures

The structure of enstatite was originally determined by Warren and Modell (1930), and many refinements have been published in subsequent years. The basic structural unit can be visualized as infinitely long SiO_3 chains ($\sim \| c$) based on SiO_4 tetrahedra sharing two vertices and having all of their apical oxygens pointing in a common direction ($\approx \| a$, or $-a$) perpendicular to the length of the chain. Neighboring chains possess apices pointing in opposite directions. The result is that an *a-c* projection consists of "plates" containing silicon and oxygen

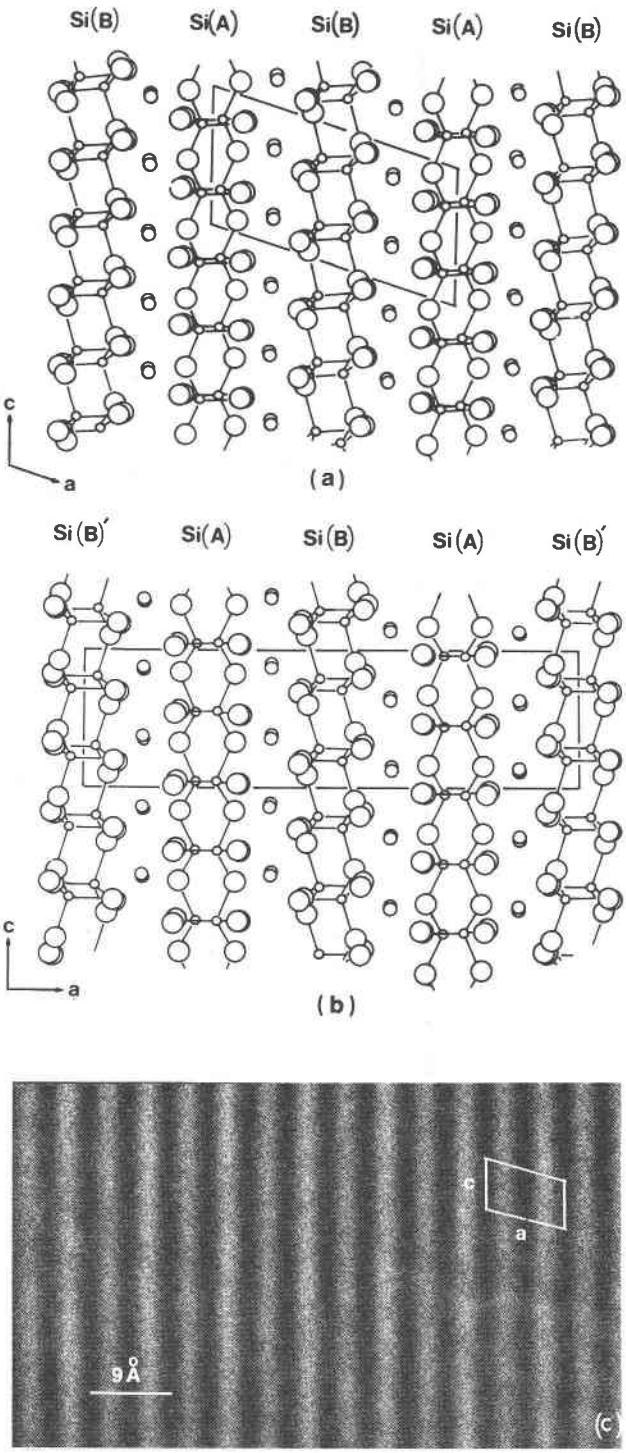

FIG. 1. Representations of the structures of (a) CLEN and (b) OREN projected on (010). The large circles represent oxygens; the small ones, silicons; and the intermediate ones, octahedrally-coordinated cations. Unit cells are outlined with solid lines (after Morimoto and Koto, 1969). (c) Electron image of synthetic CLEN showing 4.5Å fringes corresponding to the Si–O "plates."

(Fig. 1a,b). The larger cations—Mg for pure enstatite but Fe, Ca, Al, Mn for other pyroxenes—lie between the "plates", in octahedral coordination to the oxygen within the plates.

Two types of SiO_3 chains—Si(A) and Si(B) chains—alternate in CLEN (Fig. 1a) and in OREN (Fig. 1b) with the distinguishing feature that the Si(A) chains are more fully extended parallel to c (Morimoto and Koto, 1969). If twinning occurs, it is useful to distinguish between, for example, Si(B) and Si(B)′ where these chains are understood to be in a twin relationship to one another.

The chains are viewed "end-on" in a-b projections. In this instance the two types of cation sites, $M(1)$ and $M(2)$, are situated where the apices of the chains point toward and away from one another, respectively. In this case the lower electrostatic potential of the $M(2)$ sites produces lighter areas on the structure image (see Fig. 11a of Buseck and Iijima, 1974).

In the a-c structure image (Fig. 1c) the dark fringes at 4.5 Å spacings correspond to the "plates" of opposing SiO_3 chains shown in Figure 1b. At less-than-exact crystal orientations, at lower magnifications, or at improper defocussing conditions, and for thick ($> \sim$100Å) crystals, it is not possible to determine which fringes correspond to the SiO_3 "plates" and which to the intervening sites of octahedrally coordinated cations. Furthermore, under such less-than-ideal viewing conditions, the 4.5Å fringes lose their prominence and only the major periodicity along a is imaged. This is sufficient to distinguish between the 9Å spacing of CLEN (space group $P2_1/c$) and the 18Å spacing of OREN (space group $Pbca$).

Boland (1972) and Champness and Lorimer (1974) also noted the different 100 spacings but interpreted them as defects resulting from compositional differences. However, we have observed these structures in Ca-free synthetic enstatites. In the following discussion we assume that the differences we observe reflect structural variations and that the 9Å and 18Å spacings represent CLEN and OREN respectively. When their concentrations are great enough, the electron diffraction patterns confirm this identification.

Another interesting possibility regarding the 9Å "plates" is that they are produced by isolated regions of PEN. Although experimental data indicate that PEN is unstable at room temperature, it is conceivable that small regions surrounded by OREN could be stabilized. There is, however, no confirming evidence for this interpretation and we mention it as

an interesting hypothesis which will require further investigation.

Orthoenstatite-Clinoenstatite Polymorphism

The OREN and CLEN structures are extremely similar. In their original description of the crystallography of enstatite, Warren and Modell (1930) considered the possibility that OREN is simply CLEN twinned on (100) along the edge of each CLEN unit cell (actually along alternate SiO_3 "plates"). This possibility has been discussed over the years by a number of workers including Ito (1935), Brown, Morimoto, and Smith (1961), Smith (1969), Sadanaga, Okamura, and Takeda (1969), Morimoto and Koto (1969) and Coe (1970). The proposed twin relation, a *b* glide on (100), conforms with our electron microscope data.

A sketch of a single twin plane in CLEN is shown in *a-c* (Fig. 2a) and *a-b* (Fig. 2b) projections. The offset resulting from the *b* glide is evident in the *a-b* projection.

The basic twin relationships between the OREN and CLEN structures are shown in Figure 2c and d. Note that the repeat pattern corresponds to the sequence ... *ABABAB* ... (the nomenclature is described in more detail in the last section of this paper). One slightly confusing aspect, however, is the fact that it is convenient to view the edge of the OREN unit cell as lying between the CLEN twin planes. Thus, the sequence ... *ABA* ... (or *BAB*) is required to establish the OREN structure; the necessary 18Å periodicity may then be viewed positionally as $\frac{A}{2}B\frac{A}{2}$ (or $\frac{B}{2}A\frac{B}{2}$). It follows that OREN twins would not be predicted.

Observations and Discussion

Twinning and Polymorphism

Iijima and Buseck (1975) demonstrated that alternating light and dark bands of varying widths in enstatite electron images result from polysynthetic twinning. They show twin planes that are (a) isolated, (b) in pairs 9Å apart, and (c) irregularly spaced. Figure 3 shows similar features. In it arrow #1 points to a single twin plane, corresponding to the sketch in Figure 2a. Arrows #2, on the other hand, point to regions where two twin planes are adjacent; *i.e.*, they show separations of 9Å, which is the *a* dimension of a CLEN unit cell and the closest possible twin spacing in enstatite. These match the central part of the sketch in Figure 3c and correspond to plates of OREN a single unit cell wide in the *a* direction.

Figure 4b is the selected-area electron diffraction pattern corresponding to the crystal imaged in Figure 3. It is compared to patterns of almost pure OREN (Fig. 4a) and CLEN (Fig. 4c). Note that Figures 4a and 4c both contain minor streaking parallel to a^*; these streaks are the result of small amounts of admixed CLEN and OREN, respectively. Figure 4b has a markedly different appearance. The $h00$ reciprocal lattice row shows that the crystal is predominantly CLEN. The strong streaking parallel to a^* is due to the stacking faults, the results of physical disorder. We feel that the explanation as twin planes is crystallographically more precise than stacking faults (which include other features, such as anti-phase

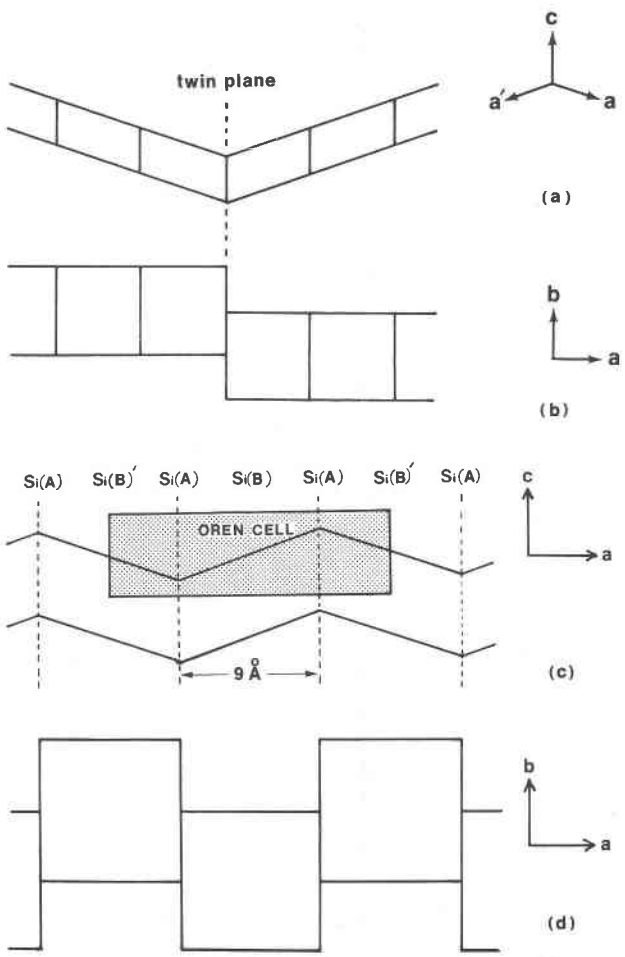

FIG. 2. Twinning in enstatite. (a) and (b) are schematic drawings of *a-c* and *a-b* projections, respectively, of CLEN. The dashed line is a twin plane. The heavy lines outline unit cells. In (a) the crystallographic axis marked *a'* applies to the right-hand twin. (c) and (d) demonstrate how repeated twinning within each of the Si(*A*) chains produces OREN.

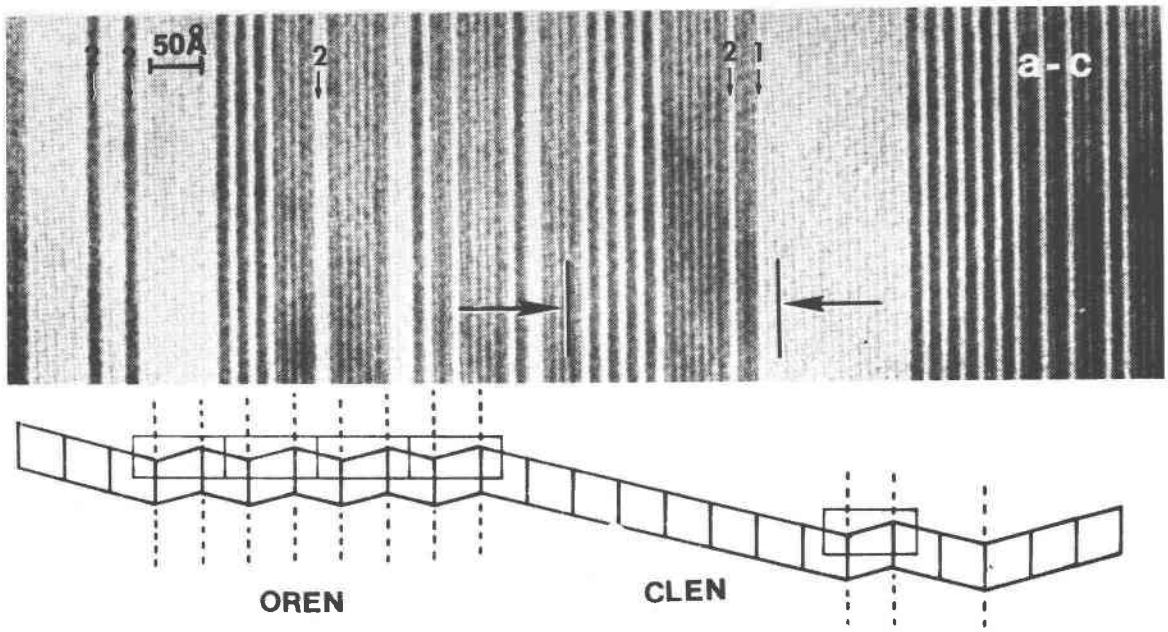

FIG. 3. Electron image of an *a-c* section of heated and quenched Bamble enstatite showing polysynthetic twinning. The vertical arrows are described in the text. The insert is a schematic representation of the structure in the area between the horizontal arrows.

boundaries) or disorder and therefore will subsequently refer to these features as twin planes.

Regions several unit cells wide of OREN within predominent CLEN are shown in Figure 3. A schematic diagram of the structure, corresponding to the areas between the large arrows, is shown at the bottom of the figure. This region can be described as $A_3BABABA_3BA_2B_3$, where the A regions of CLEN display dark contrast and the B regions are light.

Figure 5 shows an *a-b* projection of twinned

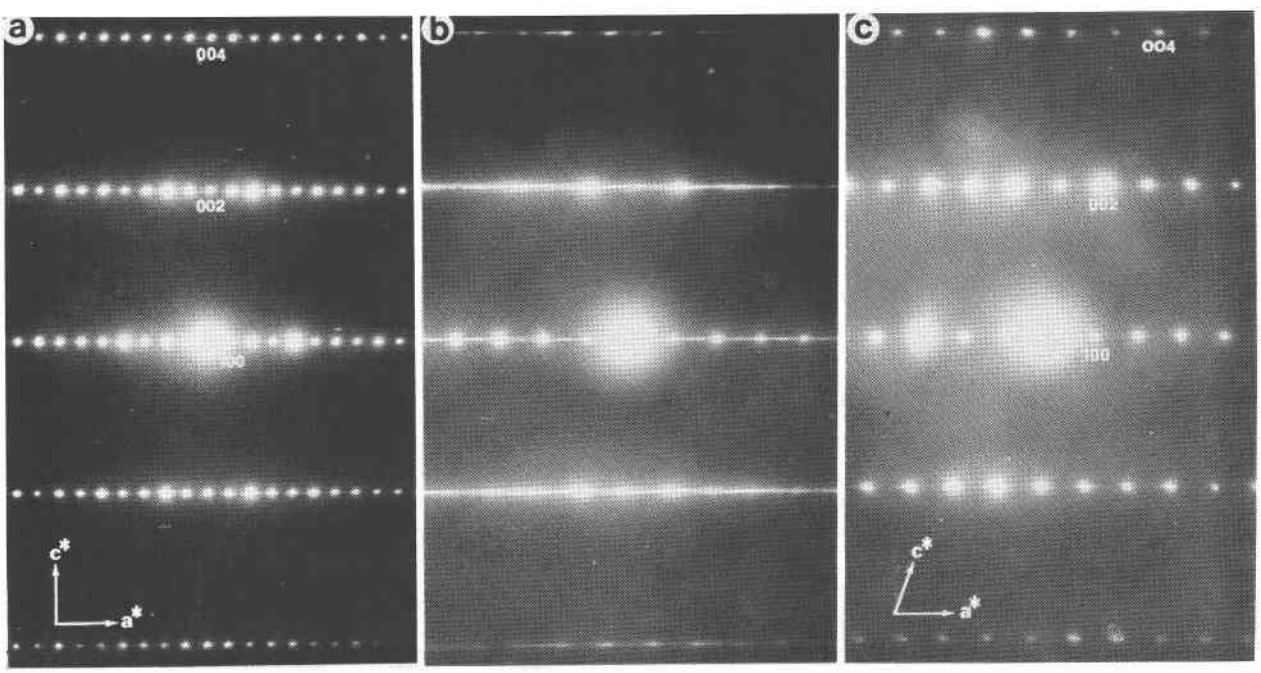

FIG. 4. Selected area electron diffraction patterns corresponding to (a) CLEN, (b) intimately intergrown OREN and CLEN, and (c) OREN.

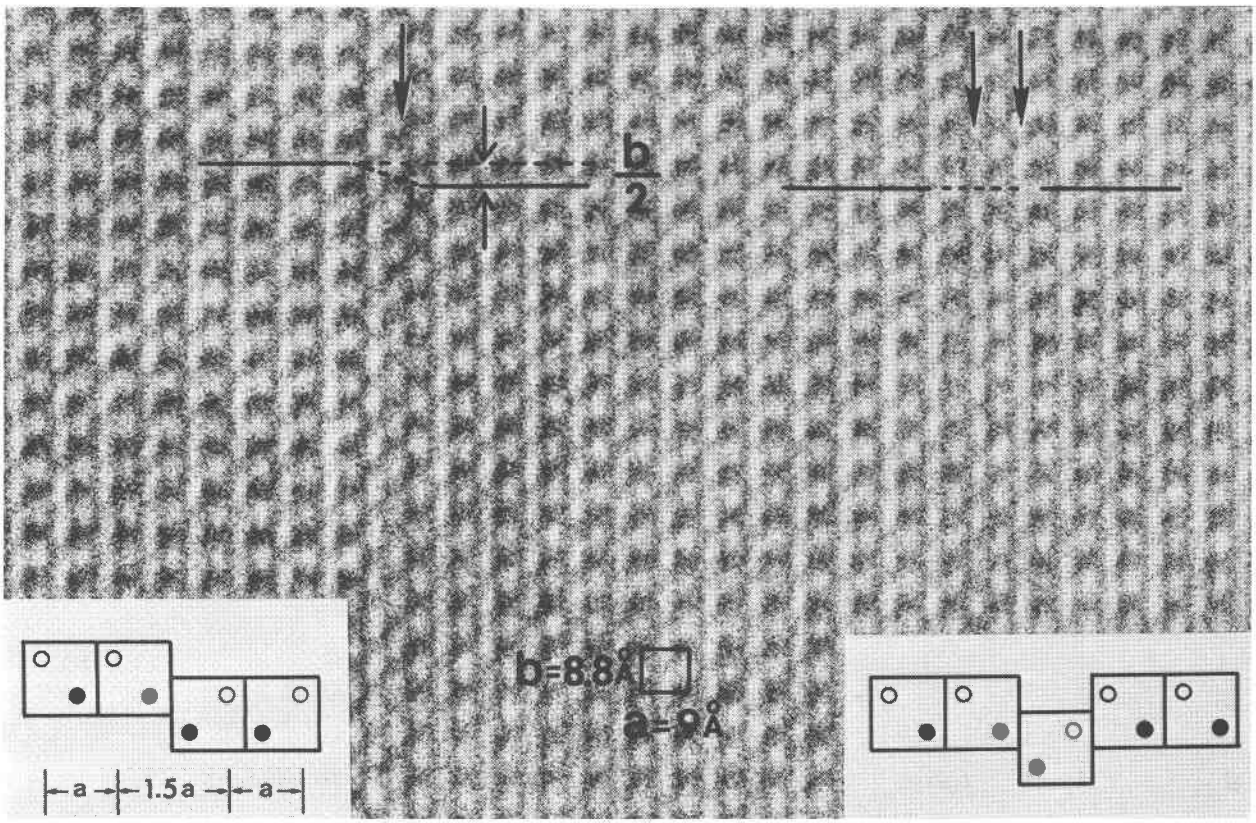

FIG. 5. *a-b* projection of Bamble CLEN showing the offset produced by *b*-glide twinning. The arrow on the left points to a single twin plane, whereas on the right there are two adjacent twin planes. A consequence is that by sighting down the picture parallel to the *a* crystallographic direction, a pronounced fringe offset is seen on the left but not on the right ($b/2 + b/2$ = coincidence). The inserts schematically illustrate the relationships. The open and closed circles distinguish between the $M(1)$ and $M(2)$ octahedral sites.

CLEN. The focussing conditions differ slightly from those in Figure 11a of Buseck and Iijima (1974), thus accounting for the slight difference in appearance (see their Fig. 6a for a more complete illustration of the dependence of the image upon focussing). A unit cell of CLEN is shown at the bottom left of Figure 5. A single twin plane occurs on the left side of the figure; the offset resulting from the *b* glide is readily visible with this orientation. The insert shows the offset schematically. A double twin, producing a unit cell of OREN, is shown on the right side of Figure 5, with its corresponding schematic insert.

An interesting feature of (100) twinning, as observed in *a-b* section, is that an extra plate, 4.5 Å ($=a/2$) wide, appears to have been added (note the spacing between corresponding fringes on opposite sides of the twin plane in Fig. 5). The explanation is related to the fact that the $M(2)$ sites are prominent in the structure image, and these sites are offset by $a/4$ from the *b*-glide plane along which twinning occurs (Fig. 5—lower left insert).

Twin Terminations and Nature of Transformation

Some of the Bamble specimens that were quenched from 1000°C or higher contain "defects" that terminate within the crystals (Fig. 6). (Similar terminated features are shown in Figure 2 of Kohlstedt and Vander Sande (1973) for unheated Mt. Albert OREN.) The (100) spacings show that some of these defects are double twins in CLEN, producing plates of OREN one unit cell wide.

Sadanaga *et al* (1969) and Coe (1970) suggested a shear transformation mechanism for the OREN → CLEN reaction. High resolution electron microscopy can be used to test their mechanism. This was done by determining the strain distribution and partial dislocation orientation surrounding OREN terminations within CLEN. The procedure differs from that conventionally used in electron microscopy and the experiments are thus described in some detail.

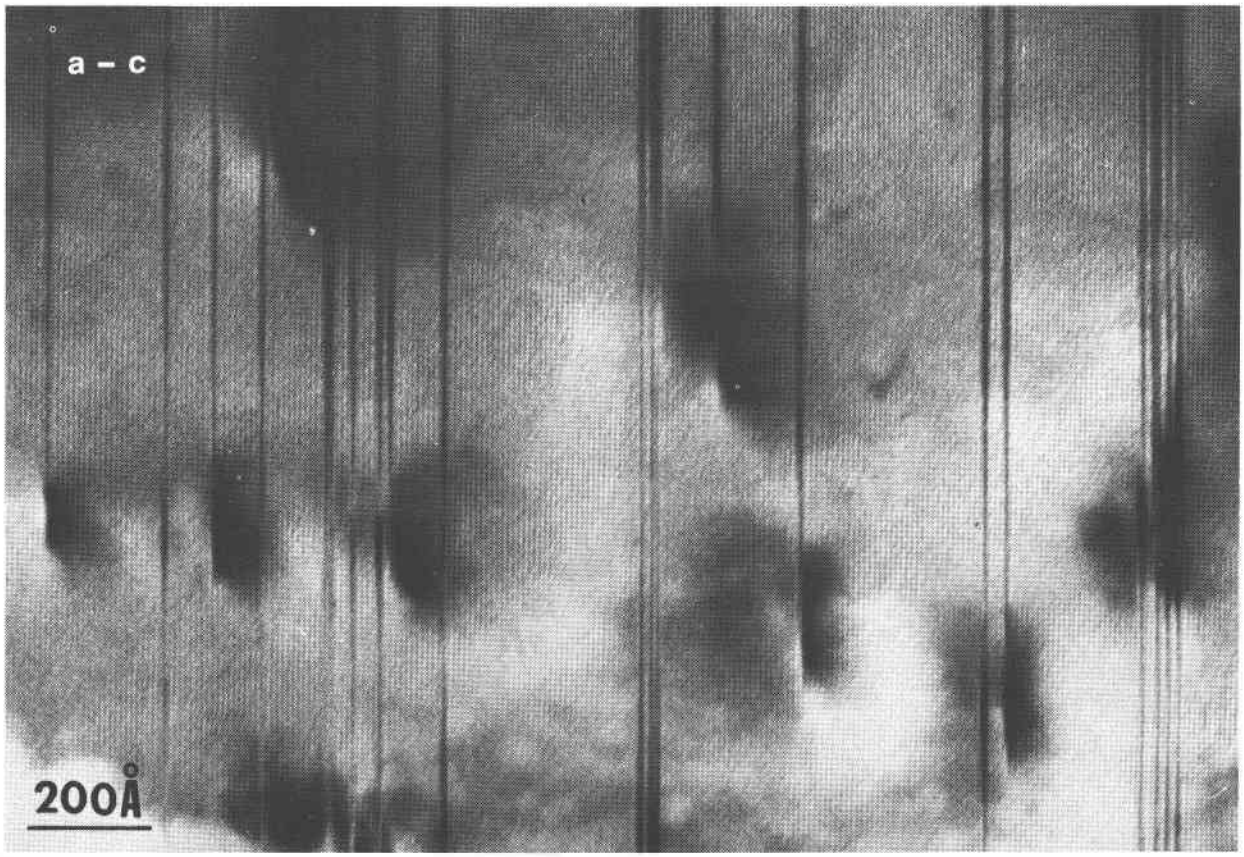

FIG. 6. Bamble enstatite containing terminated "plates" of OREN. Note the areas of dark contrast near the terminations, reflecting the strong strain fields that exist in these regions.

On the electron photomicrographs a characteristic asymmetrical dark area, indicating a strain field, occurs near the partial dislocations separating the OREN from CLEN. Tilting a wedge-shaped crystal containing a terminated plane provides data regarding the nature of the termination. Figure 7 shows three cases of a crystal tilted around *c*: (a) the plane not truncated, resulting in a triangular aspect to the plane; (b) the plane terminated parallel to the *b* crystallographic axis, resulting in a truncated triangle (*i.e.*, a trapezoid) having its line of truncation perpendicular to the tilting axis; and (c) the plane truncated in a general direction, resulting in its appearance as a general quadrilateral.

Figure 8 shows images of twin-plane terminations taken from the same grain as shown in Figure 6. In this case the crystal was tilted 3.5° and 5°, respectively, around the *c* axis. Note the change in appearance of the termination. It is now possible to determine the orientation of the plane termination, *i.e.*, the partial dislocation separating OREN from CLEN. This turns out to be parallel to [011]. Figure 9 is a schematic drawing of such a partial dislocation.

Figure 10 is an enlargement of the top surface of the rectangle in Figure 9. It corresponds to the situation where a plate of OREN, one unit cell wide, is inserted into CLEN. The circled region is the site of the OREN "plate" termination. As there is a misfit between OREN and CLEN, the lattice will be disturbed, resulting in the development of diffraction contrast. Such contrast is prominent around each of the terminations in Figure 6.

The misfit in the vicinity of the circled region of Figure 10 can be observed by carefully viewing down the (100) planes. Note that the CLEN cell edges on opposite sides of the OREN plate are not perfectly aligned, whereas there is no deviation near the bottom of the figure, *i.e.*, where no OREN occurs. The magnitude of the mismatch parallel to [001] is $R/2$, equal to $\approx c/10$.

In order to understand the nature of the lattice distortion on an atomic scale it is useful to look at the

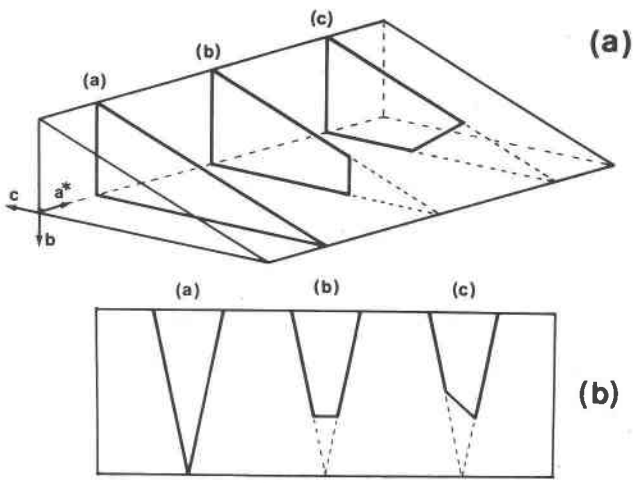

FIG. 7. (a) Planes occurring within a wedge-shaped crystal. (b) Differing aspects displayed by the planes, depending on the manner in which they are truncated.

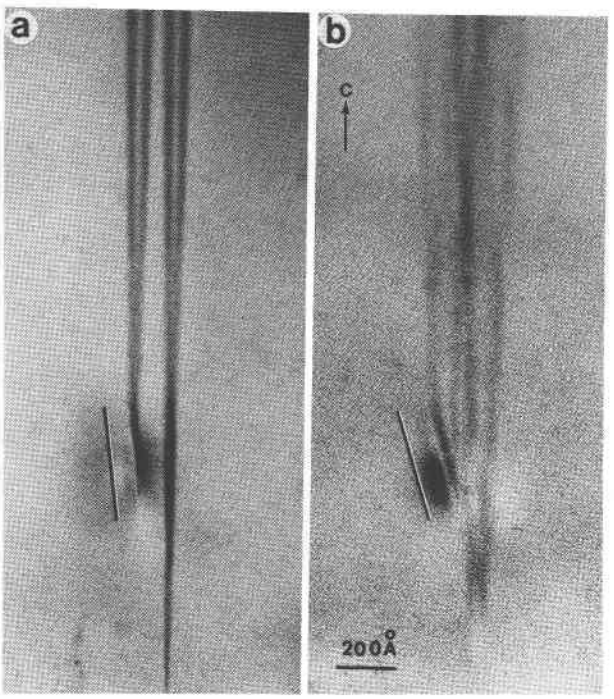

FIG. 8. Electron images of one of the OREN terminations of Figure 6. The crystal was tilted 3.5° in (a) and 5° in (b). By referring to Figure 7 the crystallographic orientation of the termination can be determined.

OREN-CLEN boundary in detail. Attention will be focussed on the positions of Si atoms along a (100) OREN-CLEN margin, for example along *stu* in Figure 9. Following the nomenclature of Smith (1969) and Morimoto and Koto (1969), these Si atoms lie within the Si(*B*) chains. Because of the lack of an exact match between the OREN and CLEN structures, these Si atoms are displaced parallel to [001], but no Si–O bonds are broken. The sense of the displacement is opposite on opposing sides of the OREN "plate". At *t* the Si atoms will have their maximum displacements. If the total mismatch is equal to *R*, then the atoms will be positioned *R*/2 from their ideal OREN-CLEN sites. The strains will be relaxed on either side of *t*, with the degree of relaxation increasing with distance from *t*.

Figure 11a shows a schematic sketch of the strain distribution, *i.e.*, the displacement of the Si atoms along the line *stu*. (It also approximates the form of the strain distribution parallel to *a**. This strain field is centered around the dislocation along the CLEN-OREN boundary.) Figure 11b shows the rows of Si atoms in the plane *stu–s't'u'* of Figure 9. The dashed, nearly vertical lines show the ideal locations of the Si atoms in CLEN; the dotted, nearly vertical lines show the ideal locations for OREN; the solid lines indicate the true positions. In other words, looking down *a**, the rows of Si atoms are rotated counterclockwise by the distortion. The deviations between the solid and broken lines are proportional to the displacements resulting from the lattice strain originating at the OREN-CLEN (001) margin. This margin is the site of the dislocation, is parallel to [011], and is the location of maximum displacement. Figure 11c shows the strain distribution along *s't'u'*; it is, of course, offset parallel to [001] from the distribution in Figure 11a.

The displacement of the Si atoms along *vwx* of Figure 10 or in plane *vwx-v'w'x'* of Figure 9 is opposite to that along *stu* and in *stu–s't'u'*. In other

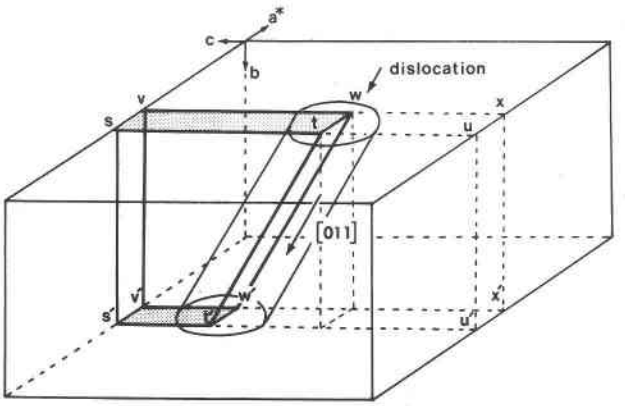

FIG. 9. Schematic block diagram of an OREN "plate" (*stwv-s't'w'v'*) terminating within CLEN, corresponding to Figure 6. The partial dislocation at the termination is parallel to [011] and the strain field surrounding it is sketched as a tilted cylinder.

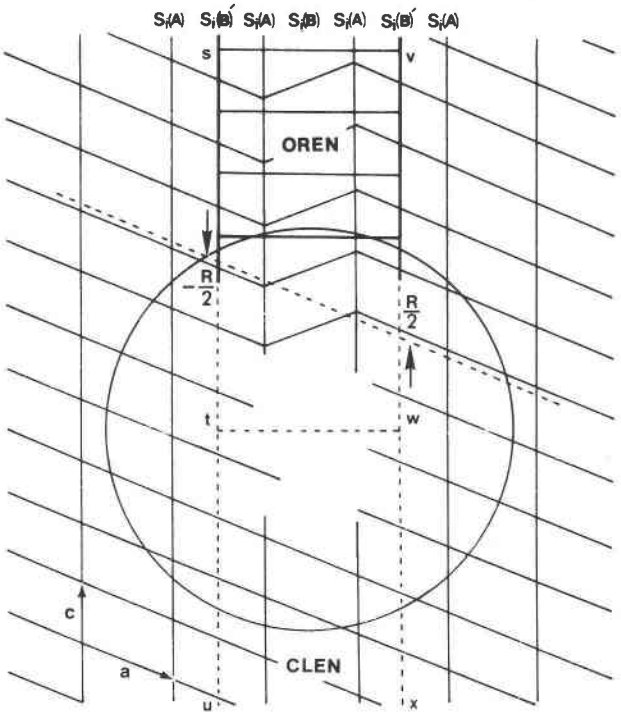

FIG. 10. Sketch of the upper (a^*-c) surface of the block diagram in Figure 9. The positions of the SiO_3 chains are shown at the top. The strain field at the OREN termination is outlined by a circle. The offset along the bounding Si(B)' chains of the OREN are indicated by the vectors $R/2$.

words, looking down the a^* axis, the rows of Si atoms are rotated counterclockwise in plane stu–$s't'u'$ and clockwise in vwx–$v'w'x'$. Yet another way of describing the relationship is to note that the Si displacements in the plane vwx–$v'w'x'$ are described by the mirror image of Figure 11b.

The preceding model describing the displacement of the Si atoms can be tested using the electron microscope. Figures 12a, b, and c show dark field images, obtained by beam tilting, using operating vectors $g = 20\bar{2}$, $\bar{5}00$, and $\bar{1}02$, respectively. Actually, because of the small reciprocal spacings, the dark field aperture also encloses several other reflections. Note, in particular, the shifts in contrast that are developed around the terminations. Contrast is enhanced if the beam is tilted in one direction around or close to a^* and the contrast almost disappears if the beam is tilted in the opposite direction.

The position of the incident electron beam, relative to the crystal, can be viewed by noting the arrows labeled i_1, i_2, and i_3 in the center of Figure 11b. In the case of i_1 the electron beam has been rotated around a direction that is very close to a^*. The beam is almost parallel to the planes of displaced Si atoms near to the OREN-CLEN (001) margin. In this instance the Si planes satisfy the Bragg condition for diffraction, and consequently the image of the region of the termination brightens. More precisely, because the Si atoms are displaced in opposite directions on either side of the OREN plate, the image (Fig. 12a) is bright on one side (the left) of the termination and in dark contrast on the other (the right).

The opposite situation is shown by tilting the electron beam parallel to i_3 (Fig. 11b). In this case the beam is far from parallel to the rows of displaced Si atoms shown in Figure 11b and so would be far from the Bragg condition. Thus the crystal would show dark contrast for that side of the OREN "plate." This situation is shown in Figure 12c, where only the right side of the termination (opposite to that in Fig. 12a) is in bright contrast. For that side the displaced Si atoms fulfill the Bragg condition, whereas on the left they do not, explaining the dark contrast on the left side.

If the beam is tilted within the a^*-b plane, the contrast adjacent to the termination will be symmetrical,

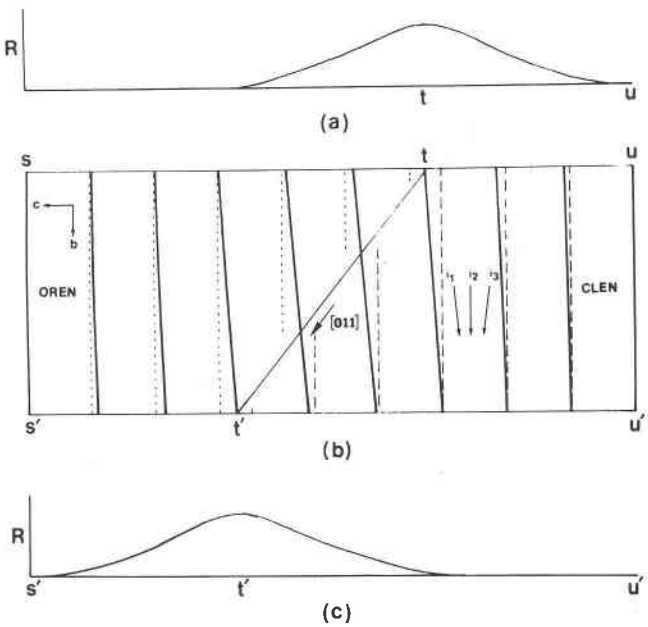

FIG. 11. The strain fields and Si atom offsets are shown in this schematic diagram along the side (b-c) of the OREN-CLEN boundary shown in Figure 9. OREN is to the left and CLEN to the right; line t-t' is the trace of the [011] dislocation. Dotted lines show the theoretical positions of Si atoms in OREN and dashed lines of Si in CLEN. The heavy tilted lines show the actual trajectories and thus displacements of the Si atoms from their idealized positions. Graphs at the top and bottom plot the strain distribution, R, versus position across the OREN-CLEN boundary.

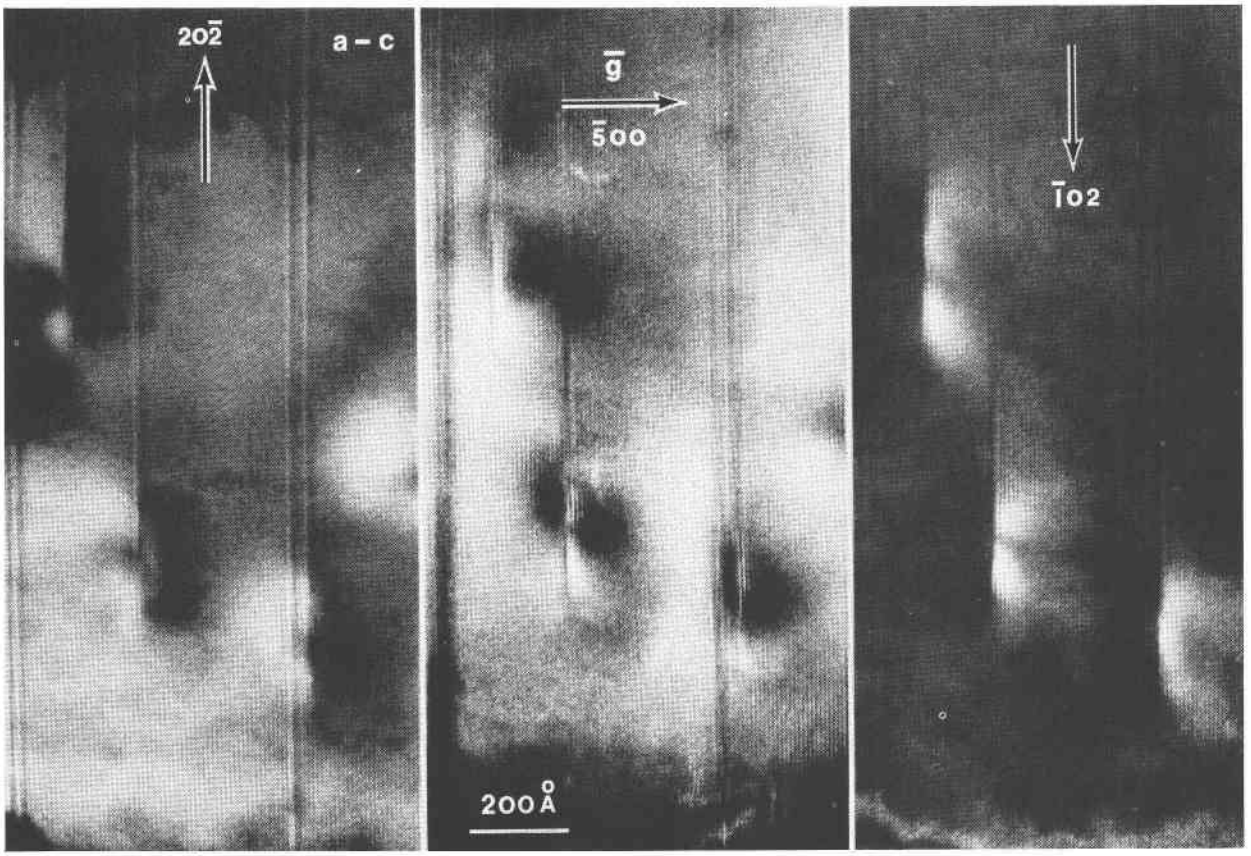

FIG. 12. Tilting experiment testing the model described in Figures 8 to 11. Terminated OREN plates are similar to those in Figure 6. These are dark field images; operating vectors 20$\bar{2}$, $\bar{5}$00 and $\bar{1}$02 have been used in (a), (b) and (c), respectively, with the electron beam tilted so that it is successively parallel to i_1, i_2, and i_3 of Figure 11. The operating vectors represent the tilting directions. Note the changes in contrast. See text for discussion.

rather than asymmetrical as in Figures 12a and c. This is because the displacement of the Si atoms is equal in magnitude (even if opposite in sign) on both sides of the termination. Because these atoms are displaced they will not produce Bragg diffraction for the same crystal orientation as the non-perturbed Si atoms located further away from the termination. Consequently a region of dark contrast is predicted on either side of the termination. Figure 12b shows an image taken with the beam tilted in the a^*-b plane; the trace of the beam is shown by i_2 (Fig. 11b). Note the symmetrical regions of dark contrast that occur on opposite sides of each of the terminations. This is in agreement with the predictions and is further confirmation of the proposed model of Si atom displacements.

It is appropriate to consider other atom displacements resulting from the OREN-CLEN transformation. In the preceding discussion we emphasized the relative displacement of the Si atoms in the Si(B)′ chains (Fig. 10) along the (100) OREN-CLEN margins. All of these displacements are parallel to c, but in opposite directions on either side of the central Si(B) chain. The cation displacement in the Si(A) chains and the intervening octahedral sites are in the same directions as in the bounding Si(B)′ chains, although of differing magnitudes. The proposed displacements are in agreement with and confirmations of the model of martensitic transformation proposed by Sadanaga *et al* (1969) and by Coe (1970).

Consistent with this model, large scale transformation of enstatite would occur by growth of one of the phases, *e.g.* CLEN, by migration through the crystal of the partial dislocations that we described above. The position of greatest lattice strain would occur in the immediate vicinity of the dislocation. Migration and phase growth would consequently serve to produce crystal relaxation.

Although the bounding Si(B)′ chains need suffer no broken bonds, this is not the case for the octahedral

cations and the central Si(B) chain. In the vicinity of the (01$\bar{1}$) bounding region between OREN and CLEN, the required atomic shifts produce bond breakage. The charge balance is maintained, but structural distortions produce local regions, particularly in the octahedral sites, that result in relatively more open sites. These are potential sinks for large cations such as Ca. Thus, it is possible that minor Ca atoms in the original structure would migrate towards the phase boundary and stabilize it.

The extent of the hypothesized stabilization reaction is limited by diffusion rates. The diffusion constants for solid state reactions in rock-forming silicates are well known only for olivine (Buening and Buseck, 1973), and there the diffusion rates are low. However, data of Dr. Steven Huebner (personal communication, 1974) indicate that the rates are even lower for pyroxenes than olivine. Thus, it is conceivable that, in the absence of external stress, prolonged aging would be required to destroy such twin planes.

Relationship Between Twinning and Polytypism

For the following discussion it will be convenient to distinguish between CLEN twins. Complementary, twinned cells shall arbitrarily be labelled A and B.[2] Thus, the sequence in Figure 2a and b can be represented as $\cdots AAABBB \cdots$. Repeated twinning such as is shown in Figures 2c and 2d would be designated $\cdots ABABA \cdots$. Such continued repetition results in a new periodicity, AB, having an a dimension twice that of $a \sin\beta$ of CLEN, *i.e.*, 18Å. Clearly, there are a large number of twin combinations or stacking sequences that can be imagined. In instances where these sequences have not been perfectly periodic a stacking fault results. Such crystals have been referred to as "disordered" in the literature. As will be shown, such stacking faults and disorder are readily comprehensible in terms of the simple twinning model.

The possible repeat units for 1 to 9 CLEN cells that could be generated by regular twinning have been computed and are indicated in Table 1. The order indicates the number of CLEN multiples, with their respective spacings shown in column 2. The types of different CLEN combinations are listed in the third column. Because of the properties of periodic arrays, these combinations can be written in a number of ways. Thus the sequence $AAAB$ of order 4 can be shortened to A_3B, and is equivalent to BA_3, A_2BA, and ABA_2. For brevity the combinations in Table 1 are given using Zhdanov symbols (Verma and Krishna, 1966); thus, by using subscripts, A_3B can be shortened to (31). Column 4 shows the equivalencies for orders 1 through 4. Polytypes for order 4 were given in a somewhat different form by Brown *et al* (1961).

The "negative" of a given type can be generated by interchanging letters, *e.g.*, B_3A (13) is the negative of A_3B (31). Those instances where the negative is a twin are indicated with an asterisk in Table 1 (this occurs where all but one of the end members of a sequence form a symmetrical group, *e.g.* (3212)). If another combination is a twin, it is shown in paired parentheses, *e.g.* (2311)–(3211). Local nonsequential regions, consisting of single units of a lower order centered around the twin plane, will sometimes result from twinning. For the even-numbered orders there are a few combinations, *e.g.* (22) and (2211), for which the twin is identical to the original, *i.e.*, the twin does not generate a new repeat unit.

The multiplicities of types are shown in the last two columns of Table 1. Column 5 includes subtypes and

TABLE 1. Possible Polytypes for Enstatite and Other Materials Containing Two Types of Layers

(See text for discussion)

(1)	(2)	(3)	(4)	(5)	(6)
				Number of Types	
Order	Spacing (Å)	Type		Subtypes and Twins Included	Not Included
1	9	(1)*	A	2	1
2	18	(11)	AB	3	1
3	27	(21)*	A_2B	4	1
4	36	(31)*, (22)	A_3B*, A_2B_2	6	2
5	45	(41)*, (32)*, (2111)*		8	3
6	54	(51)*, (42)*, (3111)*, (33), (2211)		14	6
7	63	(61)*, (52)*, (4111)*, (43)*, (3121)*, (3112) - (2113), (2311) - (3211), (2221)*, (211111)*		20	9
8	72	(71)*, (62)*, (5111)*, (53)*, (4121)*, (4211) - (1124), (4112) - (2114), (44), (3122) - (2213), (311111)*, (3113), (3221) - (1223), (3212)*, (21211) - (111212), (211112), (211211)*, (221111)		36	17
9	81	(81)*, (72)*, (6111)*, (63), (5121)*, (5112) - (2115), (5211) - (1125), (54)*, (4131)*, (4122) - (2214), (411111)*, (4113) - (3114), (4221) - (1224), (4212)*, (4311) - (1134), (3132)*, (312111) - (111213), (3123) - (3213), (311121) - (121113), (3111112) - (211113), (311211)*, (3222)*, (3211111) - (111123), (3312) - (2133), (212112) - (211212), (211122)*, (21111111)*.		60	27

*Negative=twin
( ) - ( ) = paired twins

[2] These are arbitrary symbols, not to be confused with the Si(A) and Si(B) chains.

twins. The types unique to each order, neglecting subtypes and twins, are indicated in column 6; these unique types are the most interesting category for this study. Examples of observed pyroxene polytypes are given in Buseck and Iijima (1975).

Conclusions

We have demonstrated that high resolution electron microscopy is a useful technique for studying pyroxene polymorphism and intergrowths. Using this technique it is possible to determine structural details in the vicinity of stacking faults; such details show that these faults occur along twin planes or sets of twin planes. Rather than describing stacking faults by normal means in terms of their crystallographic orientation and displacement vectors, determined by examining equal thickness fringes, we have determined these features by simply examining lattice fringes.

The "defects" or stacking faults that have commonly been described from enstatites have been resolved as individual or sets of twin planes. When occurring periodically at 9Å intervals perpendicular to a, such twin planes produce OREN. Otherwise they produce either coherent intergrowths of OREN and CLEN or, if the spacings between twin planes are greater than 9Å perpendicular to a, they result simply in twinned CLEN.

Paired twin planes, and thus "plates" of OREN one unit cell wide, can be seen to terminate within a CLEN matrix. Tilting experiments permit the study of the distribution of stress fields surrounding the terminations. This, in turn, provides information regarding the nature of the martensitic OREN → CLEN transformation mechanism. The features we observe are consistent with the models of Sadanaga *et al* (1969) and Coe (1970).

The termination zone at the end of a plate of OREN within a CLEN matrix is a partial dislocation lying parallel to [011]. It is the center of a significant strain field. Adjacent Si atoms in the Si(A) chains are displaced, but the Si–O bonds remain unbroken across this zone. This is not the case for the central Si(B) chain, or for the octahedrally coordinated cations. It is in this region of broken octahedral bonds that "foreign" cations, some of which may be larger than Fe and Mg, can enter the structure and thereby stabilize the termination zones. Otherwise, the dislocations will migrate through the structure, accelerating the transformation of OREN to CLEN or vice-versa.

Acknowledgments

Helpful discussions were held with many people, including Drs. C. W. Burnham, R. Coe, J. Cowley, J. Farmer, J. Holloway, P. B. Moore, N. Morimoto, F. Okamura, and J. Smyth. We also wish to thank the following for their help at various stages: J. Armstrong, E. Holdsworth, L. Pierce, and J. Wheatley. Meteoritic specimens were obtained from the Center for Meteorite Studies at Arizona State University; terrestrial samples were given us by Drs. Holloway and Smyth. Financial support was provided by National Science Foundation grants GA25701 and DES74-22156 from the Earth Sciences Section and GH3667, a National Science Foundation facility grant for electron microscopy.

References

Boland, J. N. (1972) Electron petrography of exsolution in an enstatite-rich orthopyroxene. *Contrib. Mineral. Petrol.* **37,** 229–234.

Brown, W. L., N. Morimoto, and J. V. Smith (1961) A structural explanation of the polymorphism and transitions of $MgSiO_3$. *J. Geol.* **69,** 609–616.

Buening, D. K., and P. R. Buseck (1973) Fe-Mg lattice diffusion in olivine. *J. Geophys. Res.* **78,** 6852–6859.

Buseck, P. R., and S. Iijima (1974) High resolution electron microscopy of silicates. *Am. Mineral.* **59,** 1–21.

———, and ——— (1975) High resolution electron microscopy of enstatite II: Geologic applications. *Am. Mineral.* **60,** 771–784.

Champness, P. E., and G. W. Lorimer (1973) Precipitation (exsolution) in an orthopyroxene. *J. Mater. Sci.* **8,** 467–474.

———, and ——— (1974) A direct lattice-resolution study of precipitation (exsolution) in orthopyroxene. *Phil. Mag.* **30,** 357–365.

Coe, R. S. (1970) The thermodynamic effect of shear stress on the ortho–clino inversion in enstatite and other coherent phase transitions characterized by finite simple shear. *Contrib. Mineral. Petrol.* **26,** 247–264.

———, and W. F. Müller (1973) Crystallographic orientation of clinoenstatite produced by deformation of orthoenstatite. *Science,* **180,** 64–66.

Iijima, S. and P. R. Buseck (1975) High resolution electron microscopy of unit cell twinning in enstatite. In *Applications of Electron Microscopy in Mineralogy,* H. R. Wenk, Ed., Springer-Verlag, Heidelberg.

Iijima, S., and P. R. Buseck (1973) High resolution electron microscopy of ortho- and clinoenstatite. (abstr.) *Geol. Soc. Am. Abstr. Programs,* **5,** 679.

Ito, T. (1935) On the symmetry of the rhombic pyroxenes. *Kristallografiya,* **90,** 151–162.

Kohlstedt, D. L., and J. B. Vander Sande (1973) Transmission electron microscopy investigation of the defect microstructure of four natural orthopyroxenes. *Contrib. Mineral. Petrol.* **42,** 169–180.

Lally, J. S., R. M. Fisher, J. M. Christie, D. T. Griggs, A. H. Heuer, G. L. Nord, Jr., and S. V. Radcliffe (1972) Electron petrography of Apollo 14 and 15 rocks. *Proc. 3rd Lunar Sci. Conf., Geochim. Cosmochim, Acta Suppl. 3,* **1,** 401–422.

MacGregor, I. D. (1974) The system $MgO–Al_2O_3–SiO_2$: Solubility of Al_2O_3 in enstatite for spinel and garnet peridotite compositions. *Am. Mineral.* **59,** 110–119.

Morimoto, N. (1975) Crystal structure and fine texture of pyroxenes. *Fortsch. Mineral.* (In press).

———, AND K. KOTO (1969) The crystal structure of orthoenstatite. *Z. Kristallogr.* **129,** 65–83.

———, D. E. APPLEMAN, AND H. T. EVANS, JR. (1960) The crystal structures of clinoenstatite and pigeonite. *Z. Kristallogr.* **114,** 120–147.

MÜLLER, W. F. (1974) One dimensional lattice imaging of a deformation-induced lamellar intergrowth of orthoenstatite and clinoenstatite [$(Mg,Fe)SiO_3$]. *Neues Jahrb. Mineral. Monatsh.* **2,** 83–88.

SADANAGA, R., E. P. OKAMURA, AND H. TAKEDA (1969) X-ray study of the phase transformation of enstatite. *Mineral. J.* **6,** 110–130.

SMITH, J. V. (1969) Crystal structure and stability of the $MgSiO_3$ polymorphs: Physical properties and phase relations of Mg,Fe pyroxenes. *Mineral. Soc. Am. Spec. Pap.* **2,** 3–29.

SMYTH, J. R. (1971) Protoenstatite: a crystal structure refinement at 1100°C. *Z. Kristallogr.* **134,** 262–274.

——— (1974) Experimental study on the polymorphism of enstatite. *Am. Mineral.* **59,** 345–352.

VANDER SANDE, J. B., AND D. L. KOHLSTEDT (1974) A high-resolution electron microscopy study of exsolution lamellae in enstatite. *Phil. Mag.* **29,** 1041–1049.

VERMA, A. R., AND P. KRISHNA (1966) *Polymorphism and Polytypism in Crystals.* J. Wiley and Sons, 341 p.

WARREN, B. E., AND I. MODELL (1930) The structure of enstatite. *Z. Kristallogr.* **75,** 1–14.

WARNER, R. D., AND W. C. LUTH (1974) The diopside-orthoenstatite two-phase region in the system $CaMgSi_2O_6$. *Am. Mineral.* **59,** 98–109.

Manuscript received, August 19, 1974; accepted for publication, April 17, 1975.